Proc. Nat. Acad. Sci. USA
Vol. 70, No. 12, Part I, pp. 3423–3427, December 1973

Scanning Transmission Electron microscope Studies of Deep-Frozen Unfixed Muscle Correlated with Spatial Localization of Intracellular Elements by Fluorescent X-Ray Analysis

(nondispersive x-ray analysis/cryobiology)

MARVIN BACANER, JOHN BROADHURST, THOMAS HUTCHINSON, AND JOHN LILLEY*

Departments of Physiology, Physics, and Chemical Engineering–Materials Science, University of Minnesota, Minneapolis, Minn. 55455

Communicated by Maurice B. Visscher, July 18, 1973

ABSTRACT **Thin sections of deep-frozen unfixed muscle were studied in a scanning electron microscope modified for transmission imaging and equipped with a "cryostage" for vacuum compatibility of hydrated tissue. With an energy-dispersive x-ray analysis system, intracellular atomic species in the scan beam path were identified by their fluorescent x-rays and spatially localized in correlation with the electron optical image of the microstructure. Marked differences are noted between the ultrastructure of deep-frozen hydrated muscle and that of fixed dehydrated muscle. In frozen muscle, myofibrils appear to be composed of previously undescribed longitudinal structures between 400–1000 Å wide ("macromyofilaments"). The usual myofilaments, mitochondria, and sarcoplasmic reticulum were not seen unless the tissue was "fixed" before examination. Fluorescent x-ray analysis of the spatial location of constituent elements clearly identified all elements heavier than Na. Intracellular Cl was relatively higher than expected.**

The present body of knowledge relating the microstructure and physiologic function of muscle is based primarily on (*1*) electron microscope studies of fixed tissue, dehydrated so as to be compatible with the vacuum required for electron optical imaging and (*2*) concepts of excitation and contraction based on indirect assessments of transcellular gradients and fluxes of ions of certain elements. Many problems remain unresolved because (*1*) changes in microstructure by fixation and preparation of tissue for electron microscopy have not been related to its morphology in the living state, and (*2*) there is no direct method to measure concentration and localization of intracellular elements at functionally important sites within the living cell in association with changes in functional state without prior distortion by fixation and/or dehydration.

To reconcile uncertainties in morphology related to tissue preparation and test some of the data and assumptions involved in indirect estimates of the concentration of intracellular elements, we have explored a technique in which a scanning electron microscope (SEM) equipped with an energy-dispersive x-ray analysis system and "cryostage" was used as an analytic as well as visual instrument to study deep-frozen unfixed muscle. Thin sections of fresh muscle quick-frozen in a preselected physiologic state were studied in the cryostage at −100°, at which temperature the vapor pressure of ice is sufficiently low for vacuum compatability. Intracellular elements in the scan beam path were identified by their fluorescent x-rays in correlation with the electron optical image of the microstructure.

This report is an extension of preliminary abstracts (1, 2) indicating that (1) there are striking morphological differences in the microstructure of deep-frozen, unfixed, unstained hydrated muscle cells compared to those prepared by the conventional techniques of fixation, dehydration, embedding, and staining, and (2) intracellular elements heavier than sodium can be easily identified and spatially resolved within the ultrastructure of a single cell by their fluorescent x-rays.

EQUIPMENT AND METHODS

Tissue Preparation and Examination. To immobilize diffusible substances it is essential that movement be abruptly stopped and solutes fixed in place throughout the period of analysis. This we approached by ultrarapid freezing of small blocks of tissue on liquid-nitrogen-cooled copper (−193°). A cryostage was designed and fabricated to fit into the SEM so that deep-frozen thin tissue sections could be kept at or below −100° during observation and analysis. At such temperatures the vapor pressure of ice is sufficiently low so that sections of the cold tissue can be examined directly in the SEM at a vacuum of 10^{-5} torr without water loss. Present methods of preparing vacuum-compatible specimens of tissue—such as fixation, dehydration, and epoxy embedding; freeze substitution; or freeze drying—all involve removal of water. And, because there is considerable movement of solute associated with dehydration, these could not be used.

It was essential to maintain the frozen, thin sections in a dry atmosphere below −85° at all times, in order to preclude solute movement, water loss, and surface frosting. Prepared specimens were stored and transfered to the precooled SEM cryostage with a cartridge transfer system, holding chamber, and dry box (Fig. 1).

To obtain sufficient contrast in the electron optical images of a thin section of tissue, the normal reflected electron imaging operation of the SEM was converted to transmission imaging—causing it to function as a transmission scanning electron microscope. The contrast obtained in unstained unfixed tissue was enhanced by partial dark-field techniques that were developed for this purpose. A detailed description of the cryostage and transfer system and transmission imaging technique will be reported separately (16).

X-Ray Analysis. In the SEM, a 20 keV electron beam focused to a small spot, about 75 Å in diameter, is scanned

Abbreviation: SEM, scanning electron microscope.

* Alphabetical order.

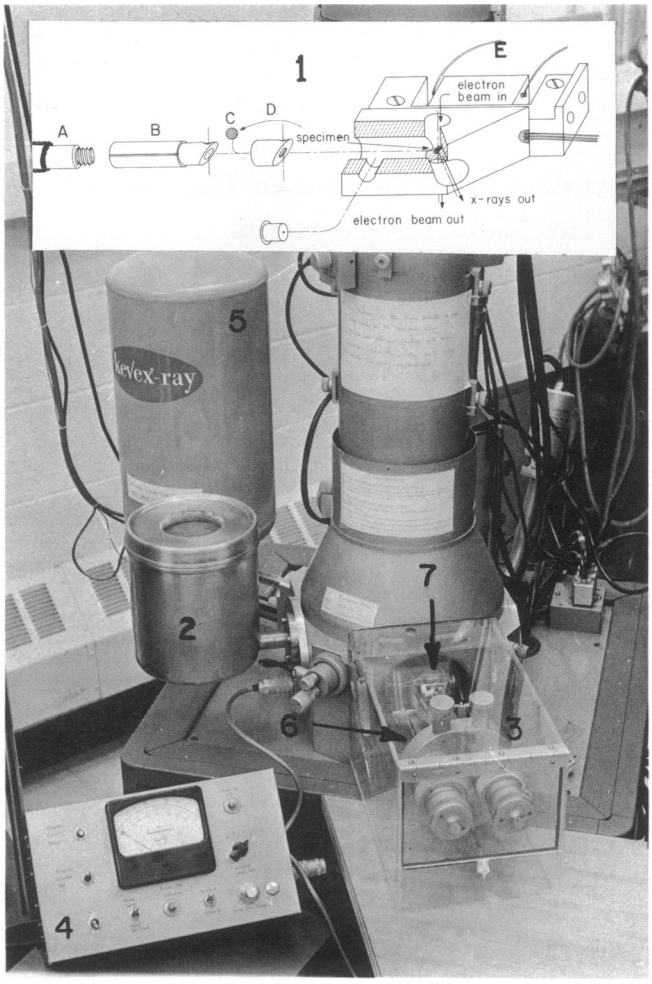

FIG. 1. Scanning Electron microscope with x-ray detection system and cold stage. (*1*) *Insert:* Cold stage and transfer system: *A*. transfer rod, *B*. grid cartridge, *C*. grid, *D*. cartridge cap, *E*. cold stage. (*2*) Cold stage dewar flask. (*3*) Plastic dry box. (*4*) Cold stage controller. (*5*) X-ray detection dewar flask. (*6*) Stage drawer. (*7*) Cold stage in position.

over a specified rectangular area of the specimen. The area can be selected by appropriate magnification settings or by selected spot or line scans. Bremsstrahlung and fluorescent x-radiation are generated by the interaction of the primary beam with the atomic constituents of the biological target. Fluorescent x-rays are produced when the incident radiation excites inner shell electrons of the elements in the specimen. When the resulting electron vacancy is refilled from a higher shell an x-ray photon is emitted whose energy is characteristic of the element and the shell from which it was displaced.

Scattered and knock-on electrons are spread out in a cone about the primary beam direction. Thus, in a thick sample, the source of fluorescent x-rays covers a relatively large region (about 5 μm for 20 keV incident energy). To minimize this effect, it was necessary for us to use thin tissue sections. The spatial resolution of the x-rays then is limited by the thickness of the target tissue (typically 1000 Å).

The x-radiation was received by a 10 mm^2 Li–Si detector (Kevex Corp.) positioned a few mm from the bombarded tissue. The detector has a resolution of 150 eV at 4 keV and a threshold of about 0.9 keV. All observable peaks corresponding to neighboring elements could be identified separately, and so, in principle, this instrument, coupled to a pulse height analyzer, allows all elements in the sample heavier than sodium to be analyzed simultaneously and correlated spatially with the electron image of the microstructure.

Procedure. Rabbits were anesthetized with a solution of pentobarbital (15 mg/kg) and valium (5 mg). The psoas muscles were exposed and with a dissecting microscope a small bundle of muscle fibers about 0.5 mm in diameter was dissected free. Two fine threads were tied about 3 mm apart and the muscle cut free just distal to the threads. The muscle bundle was mounted on a specially designed cylindrical copper chuck (4 mm in diameter by 1.2 cm long) with a fine groove cut across one end, slightly beveled to center the muscle longitudinally for sectioning. The threads were passed under spring wires on each side of the center groove to hold the muscle at either rest length or under some degree of stretch. The chuck fixed in a plastic holder was passed through guides until the specimen gently touched a pure copper block cooled to liquid nitrogen temperature (*3*).

Frozen thin sections were cut with an ultramicrotome (Ivan Sorvall MT2B) fitted with a frozen thin-sectioning attachment modeled after the unit described by Christianson (*3*). Cooling to −85° was achieved by streaming vapor from liquid nitrogen into the base of a shroud surrounding the cutting area at a rate appropriate to keep the stable preset temperature. The frozen tissue was trimmed (in the shroud) to leave a wedge-shaped rectangular region 0.10–0.15 mm on a side. Sections 1000–1400 Å thick were cut with a fresh glass knife, and placed on a 300-mesh copper grid. A second 100-mesh copper grid was placed on top of the first. The two grids were cold-welded together with the tissue sections between them and placed in a precooled cartridge designed for transfer to the cryostage in the SEM (Fig. 1, *insert*). This transfer was accomplished by first withdrawing the cartridge into the liquid-nitrogen-cooled transfer cylinder of a transfer rod that forms a cold trap protecting the specimen during transport of the cartridge (Fig. 1, *insert*). To insert the cartridge into

TABLE 1. *Regional x-ray scans**

Region	Concentrations relative to sulfur†				Ratio	
	P	Cl	K	Ca	K/Cl	Ca/K
			Experiment 1			
Area scan 1	1.2	0.8	2.4	0.3	3.0	0.1
Area scan 2	1.2	0.9	1.7	0.5	2.0	0.3
			Experiment 2			
On Z-zone	0.2	1.6	1.4	0.7	0.9	0.5
Off Z-zone	0.2	2.7	2.3	0.8	0.9	0.4
			Experiment 3			
On Z-zone	Trace	1.0	1.4	1.3	1.4	0.9
Off Z-zone	0.16	0.9	1.2	0.9	1.3	0.7
			Experiment 4			
Rabbit serum	0.2	3.8	0.4	0.1	0.1 (Na/Cl = 1.1)	0.2

* Corrected for overall detector efficiency.

† All element concentrations have been normalized to a value of 1 for sulfur.

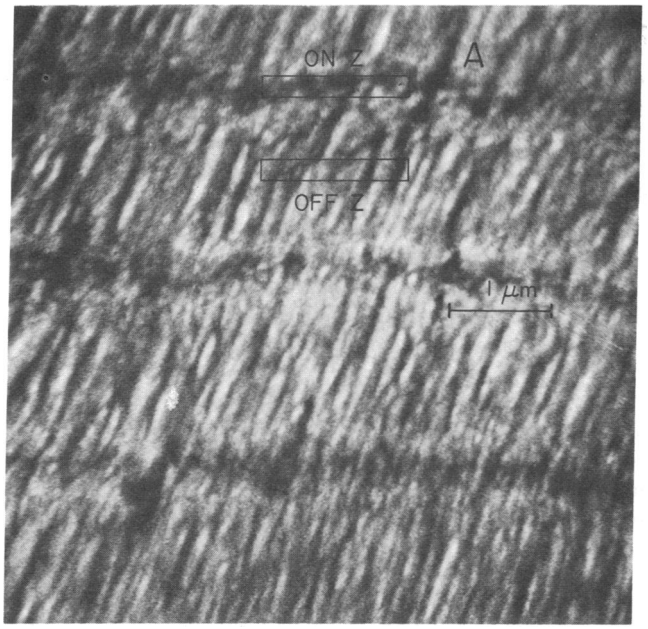

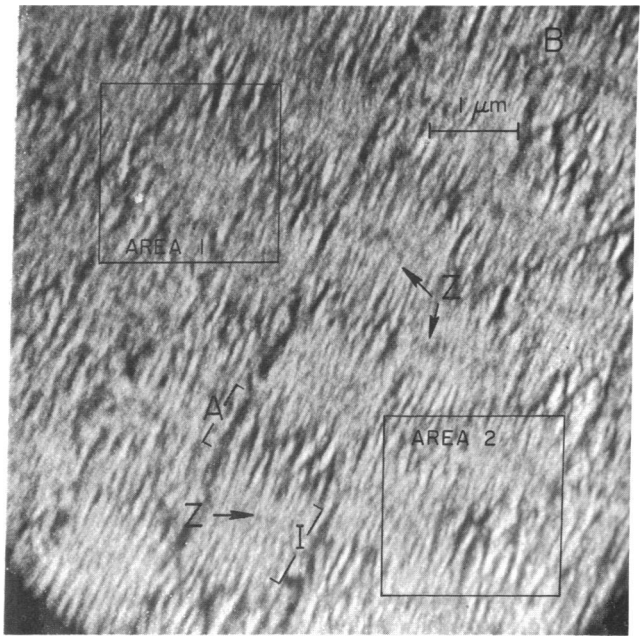

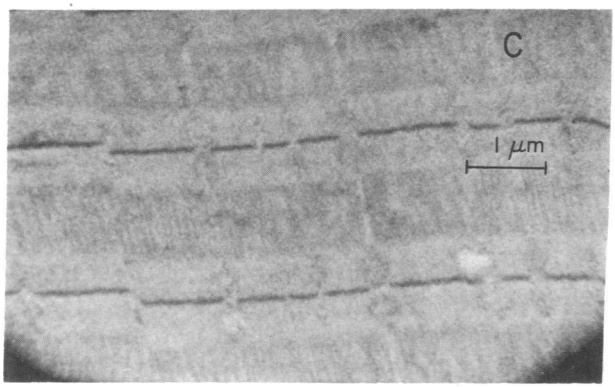

FIG. 2. Transmission SEM micrography of thin (1000 Å) longitudinal sections of rabbit psoas muscle. (*A*) Unfixed, unstained specimen frozen at rest length viewed in frozen state. Microstructure consists of about 1000-Å elements ("macromyofilaments") which run through electron-dense "Z-zones" without interruption. (*B*) Same as *A* except muscle was stretched 20% prior to freezing. Myofibrils (about 1 μm) with darks bands ("A-zones") composed of about 1000-Å macromyofilaments which become thinner (about 400–600 Å) and more densely packed in the lighter "I-zones." *Arrows* point to "Z-zones." *Boxes* outline areas similar to those scanned for fluorescent x-ray analysis (Table 1). (*C*) Muscle was deep-frozen and thawed in warm fixative (37°) before conventional preparation, epoxy-embedding, and staining. A-, I-, and Z-bands and thick filaments (150 Å) are observed, indicating that freezing does not alter conventional ultrastructure.

microscope cryostage, which was precooled to about −100°, the process was reversed. The cartridge was transferred to the cryostage through a dry box that was kept moisture free with a continuous stream of dry nitrogen gas flowing out through the microscope column and the cartridge was pushed out of the hollow cylinder. The transfer rod was inserted through the dry box into the aligning keyway of the cold stage. In this position the grid was centered and oriented at 45° to the electron beam when the stage was reinserted.

RESULTS

Microstructure of Frozen Muscle. Fig. 2*A* and *B* show representative transmission electron micrographs of deep-frozen thin sections (about 1000 Å) of hydrated, unfixed, unstained skeletal muscle. Fig. 2*A* shows a longitudinal section from a group of muscle fibers frozen at rest length. Dark bands approximately 2 μm apart run transversely across the longitudinal section. The transverse striations are not sharply defined structures but rather are electron dense bands through which longitudinal elements, about 1000 Å wide, run without interruption. We term this the "Z-zone," as it appears to correspond to the Z-band of electron micrographs of tissue prepared by the usual fixation, staining, and embedding methods. The 1000 Å-wide longitudinal elements are previously undescribed structures that we have termed "macromyofilaments." Myofibrils are not apparent in this specimen of muscle at rest length.

Fig. 2*B* is a section from a muscle that was stretched to about 20% more than rest length before freezing. The typical longitudinal myofibrils of the muscle cell (about 1 μm wide) are apparent and show alternating light and dark cross-bands. The myofibrils in this section also are composed of longitudinal macromyofilaments. These are about 1000 Å wide in the dark zones (A-zone), but appear to branch and/or narrow to about 400–600 Å and become more densely packed in the lighter or I-zones. The latter may correspond to the I-bands of conventional electron micrographs of skeletal muscle. In the center of some of the I-zones slightly darker bands (Z-zones) can be observed (Fig. 2*B*, *arrow*). In some of the I-zone areas it appears that the thinner macromyofilaments are uncoiled or branched continuations of the thicker bundles of the A-zone in a basketweave pattern moving in and out of the plane of the section.

The classical components of conventional electron micrograph ultrastructure of striated muscle, thick (150 Å) and thin (60 Å) myofilaments, well-defined mitochondria, sarcoplasmic reticulum, and tubules are not seen in electron micrographs of otherwise untreated deep-frozen muscle.

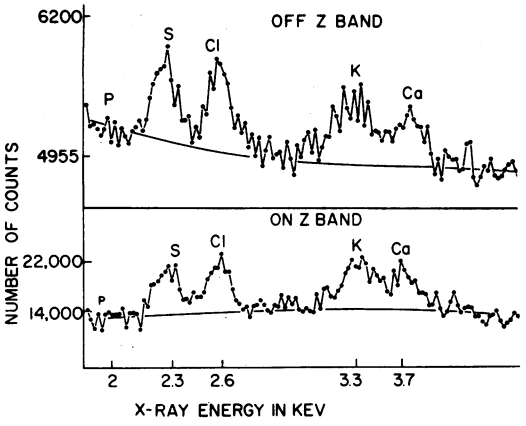

FIG. 3. Energy spectrum of fluorescent x-rays of frozen muscle bombarded with 20 keV electrons. Areas that correspond to a Z-zone (*lower* spectrum) and off Z-zone (*upper* spectrum) are similar to *boxes* outlined in Fig. 2*A*.

To determine if freezing irreversibly alters ultrastructure, we froze a series of muscles in the usual way and thawed them rapidly in warm (37°) fixative (2% glutaraldehyde + 2% paraformalin), then conventionally dehydrated, embedded in epoxy and stained (lead citrate and uranyl acetate) them. A transmission image electron micrograph taken in the SEM (Fig. 2*C*) shows that conventional A-, I-, and Z-bands are apparent, and that thick filaments (150 Å) can be resolved. Multiple studies of high resolution transmission electron micrographs of frozen-thawed and then conventionally processed psoas muscle indicate that the freezing technique employed in our studies does not produce any apparent damage to typical muscle ultrastructure. Frozen-thawed sections are indistinguishable from unfrozen controls.

Regional X-Ray Analysis of Elemental Composition of Skeletal Muscle. Relative intracellular concentrations of phosphorus, sulfur, chlorine, potassium, and calcium in various regions of rabbit psoas muscle cells are shown by the x-ray energy peaks in Fig. 3 and 4, and the relative numerical values are presented in Table 1.

As the "Z"-zone seen in Fig. 2*A* appears to be an electron-dense region rather than a structural element, it may represent a region in which the heavier elements are concentrated. The two x-ray energy spectra (Fig. 3) were generated by scanning narrow areas on and off the "Z"-zone as shown by the areas outlined in Fig. 2*A* (Exp. 2, Table 1). In the stretched muscle two neighboring areas (about 4 μm^2 each) thought to represent similar groups of sarcomeres in the same cell were scanned. The x-ray spectra (Fig. 4) correspond to area scans 1 and 2 (Fig. 2*B*). Intracellular concentration of elements in rabbit psoas muscle is given in Table 1, which includes a comparison with assumed relative extracellular element concentration of serum as reflected by x-ray analysis of a thin film of rabbit serum. Relative concentrations have been corrected for overall detector efficiency established by an analysis of thin films of pure chemical compounds.

Apparently there is a relatively large amount of chlorine inside the muscle cell. While the relative concentration of intracellular chlorine is considerably less than in serum, (Table 1), it is much higher than anticipated (4).

There is regional heterogeneity in the relative concentration of elements inside the cell. It was expected that *areas 1* and *2* (Figs. 2*B* and 4, Table 1) would have similar relative concentrations since they are scans from neighboring groups of sarcomeres within the same cell. Nevertheless there are significant differences in K/Cl and K/Ca ratios. There also are regional differences suggested by the observation of more calcium relative to potassium in the Z-zone than in areas off the Z-zone (Figs. 2*A* and 3, Table 1).

There is also variability in concentration and localization of phosphorus between specimens (Figs. 3 and 4, Table 1). There are large phosphorus peaks in the larger general areas scanned (Fig. 2*B*), while phosphorus peaks are small in narrow area scans focused on and off the Z-zones (Fig. 3, Table 1).

DISCUSSION

The observed differences in morphology and intracellular ion composition do not appear to fit into current concepts relating muscle structure and function. Some tentative attempts to reconcile the observations with existing information seem appropriate.

Morphological Considerations. The previously unreported (400–1000 Å) macromyofilaments are the dominant feature of electron microstructure of frozen rabbit psoas muscle. Macromyofilaments remain when the frozen tissue is vacuum dried by warming the cryostage. We have also observed this about 1000 Å element in SEM reflection electron micrographs of dried frog skeletal and beetle flight muscle (unpublished observations). The failure to observe thick and thin myofilaments, mitochondria, and sarcoplasmic reticulum could be attributed to insufficient contrast in unstained hydrated tissue, but not by the limits of resolution of the SEM. That thick filaments (about 150 Å) are within the resolving power of our SEM is clear from Fig. 2*C*, which also gives evidence that our technique of rapid freezing (and thawing) does not distort or alter the classical architecture of muscle.

It is possible that thick and thin filaments are component structures of the macromyofilaments that separate during the process of tissue preparation for electron microscopy. Tissue morphology is sensitive to the details of every step required in the processing of tissue for electron microscopy (5). There

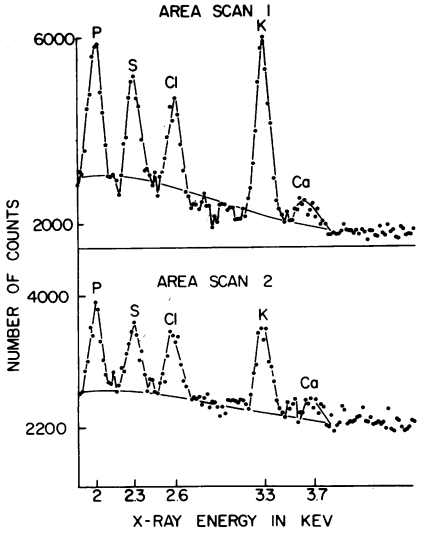

FIG. 4. Energy spectrum of fluorescent x-rays of frozen muscle bombarded with 20 keV electrons. Areas scanned correspond to *boxes* outlined in Fig. 2*B*.

is general agreement that crosslinking of proteins occurs in fixation; alteration of protein structure by alcohol denaturation occurs during dehydration; substitution of epoxy for alcohol and heavy metal staining systematically distort the native state of the tissue (5, 6).

To determine the effect of fixation itself on morphology of frozen muscle independent studies were carried out. Muscles mounted on chucks were fixed overnight, then frozen in the usual way and examined in the frozen state. Fixation intensified electron density and banding, markedly widened the distance between myofibrils, and made quite apparent mitochondria and sarcoplasmic reticulum previously unseen. In our opinion the electron micrograph morphology of unfixed deep-frozen muscle (Figs. 2*A* and *B*) reflects a much closer approximation to the living state than does conventionally fixed and processed tissue (Fig. 2*C*). It remains for continued studies to reconcile and explain the observed differences and to consider the structural implications in the contractile process.

Assessment of Intracellular Ion Composition. There is considerable uncertainty about the ionic composition of the cell interior. Current estimates are indirect and based on calculations with unverified assumptions. The variability and inconsistency in estimates of extracellular volume are related to differences in compartmental distribution of extracellular markers used (7, 8). The choice of which extracellular volume to use in estimating intracellular electrolyte composition is thus arbitrary. Correlation of anatomical estimates of extracellular space with a variety of presumably impermeable and nonbinding extracellular markers is not good (7, 8). This is probably related to fixation and dehydration steps necessary to prepare tissue for microscopic examination.

Also, it is assumed that the monovalent intracellular ions are in free solution as though in a water-filled sac. Our data, on the other hand, indicate that it is more likely that there is intracellular heterogeneity of element distribution and perhaps binding at specific sites within the cell or membrane. Binding of ions would remove them from the electrochemical active state and preclude their influence on forces involved in electrochemical gradients (9). Selective binding would thus influence estimates of concentration and gradients for presumably freely diffusible ions.

The assumption that the extracellular compartment is a simple ultrafiltrate of serum whose ionic composition can be determined by analysis of serum also is open to question. Johnson (10) found that washout curves of a number of radioactive labeled extracellular markers from heart muscle had both fast and slow components. He postulated that there may be diffusion barriers within the extracellular compartment to account for his results. However, it would be difficult to exclude membrane binding or transmembrane movement as an alternative explanation.

We consistently observed considerable intracellular chlorine in psoas muscle. Although very little information exists on the chloride concentration in normal mammalian muscle cells, it is usually assumed that it is very low. Indeed, the chloride space still is equated with the extracellular space in most current work done in skeletal muscle (9). There is evidence, however, that frog muscle is permeable to chloride. Boyle and Conway (11) showed that when external potassium and chloride concentrations were varied over a wide range, the muscle potassium and chloride conformed with the concentrations to be predicted for a Donnan equilibrium system in which the membrane is permeable to these ions. Hodgkin and Horowicz (12) showed that frog skeletal muscle is permeable to chloride and that the chloride conductance was about twice the potassium conductance. Hutter and Noble (13) found that in the resting state, chloride ions accounted for about two-thirds of the total membrane conductance.

There is also some indirect evidence that mammalian muscle is permeable to chloride, and that chloride is normally present within the cells, from the experiments of Giebisch *et al.* (14) in which membrane potentials were measured in single fibers from perfused hindlimb preparations of cat gracilis muscle. Partial replacement of sodium chloride by sucrose caused depolarization associated with a sharp increase of potassium and lactic acid in the venous outflow. Contractions and fibrillations occurred when sulfate was substituted for chloride. These effects were thought to be a consequence of loss of intracellular chloride when extracellular chloride was lowered.

There was considerable variability of intracellular phosphorus in muscles from different rabbits. Many organic phosphate compounds are intimately linked to metabolism and, while phosphorus in some form enters cells, inorganic phosphate is so poorly diffusable that it has been used to measure extracellular space (9). A possible explanation for the variability is that intracellular phosphorus may be localized to relatively specific regions inside the cell that were outside the small areas on and off the Z-zone that were scanned.

Potential gradients sufficient to move ions through the tissue may develop along the water-ice interface during freezing. Such a phenomenon has been demonstrated to occur at low freezing rates in dilute aqueous solutions (15). The effect is reduced at high rates of freezing, and, at the ultrarapid cooling rates we employ, in which the freezing rate exceeds the self diffusion rate of water, it is unlikely that the ions will be moved significantly from their *in vivo* positions.

1. Bacaner, M., Broadhurst, J., Hutchinson, T. & Lilley, J. (1972) *Fed. Proc.* **30**, 324.
2. Bacaner, M., Hutchinson, T., Broadhurst, J. & Lilley, J. (1973) *Fed. Proc.* **31**, 373.
3. Christensen, A. K. (1971) *J. Cell Biol.* **51**, 772–804.
4. Barlow, J. S. & Manery, J. F. (1954) *J. Cell. Comp. Physiol.* **43**, 165–191.
5. Trump, B. F. & Ericsson, J. L. (1965) *Lab. Invest.* **14**, 496–595 (Symposium).
6. Rebhun, L. I. (1965) *Fed. Proc.* **24**, Part III, 5217–232.
7. Johnson, J. A. & Simonds, M. A. (1962) *Amer. J. Physiol.* **202**, 589–592.
8. Bohr, D. F. (1964) *Pharm. Rev.* **16**, 85–111.
9. Horowicz, P. (1964) *Pharm. Rev.* **16**, 193–221.
10. Johnson, J. (1955) *Amer. J. Physiol.* **181**, 263–268.
11. Boyle, P. J. & Conway, E. J. (1941) *J. Physiol.* **100**, 1–63.
12. Hodgkin, A. L. & Horowicz, P. (1959) *J. Physiol.* **148**, 127–160.
13. Hutter, O. F. & Noble, D. (1960) *J. Physiol.* **151**, 89–102.
14. Giebisch, G., Kraupp, O., Pillat, B. & Stormann, H. (1957) *Pflügers Arch. Gesamte Physiol. Menschen Tiere* **265**, 220–236.
15. Workman, E. J. & Reynolds, S. E. (1950) *Phys. Rev.* **78**, 254–259.
16. Hutchinson, T. E., Bacaner, M., Broadhurst, J. & Lilley, J. (1973) *Rev. Sci. Inst.*, in press.